UC Irvine

Title

Unusual Radar Echoes from the Greenland Ice Sheet

Permalink

Journal

ISSN

Authors

Rignot, EJ
Ostro, SJ
van Zyl, JJ
et al.

Publication Date

DOI

Copyright Information

Peer reviewed

REFERENCES AND NOTES

1. C. Miller, *Science* **252**, 1092 (1991).
2. B. Hille, *Ionic Channels of Excitable Membranes* (Sinauer, Sunderland, MA, 1992).
3. G. Yellen, M. E. Jurman, T. Abramson, R. MacKinnon, *Science* **251**, 939 (1991); R. MacKinnon and G. Yellen, *ibid.* **250**, 276 (1990); A. J. Yool and T. L. Schwarz, *Nature* **349**, 700 (1991); R. MacKinnon, *ibid.* **350**, 232 (1991).
4. For a large number of pore sequences, see M. P. Kavanaugh *et al.*, *J. Biol. Chem.* **266**, 7583 (1991). The very recently sequenced inward-rectifier K⁺ channels are quite different in structure from A-type K⁺ channels, but are highly conserved in the pore. The GYG sequence is conserved, and FLF replaces FWW. See K. Ho *et al.*, *Nature* **362**, 31 (1993); Y. Kubo, T. J. Baldwin, Y. N. Jan, L. Y. Jan, *ibid.*, p. 127. Similarly, in the very recently sequenced calcium-dependent K⁺ channel mSlo, the GYG is conserved, but VYL appears to align with the FWW. See A. Butler, S. Tsunoda, D. P. McCobb, A. Wei, L. Salkoff, *Science* **261**, 221 (1993). Abbreviations for the amino acid residues are A, Ala; D, Asp; F, Phe; G, Gly; L, Leu; M, Met; T, Thr; V, Val; W, Trp; and Y, Tyr.
5. D. A. Dougherty and D. A. Stauffer, *Science* **250**, 1558 (1990).
6. M. A. Petti, T. J. Shepodd, R. E. Barrans Jr., D. A. Dougherty, *J. Am. Chem. Soc.* **110**, 682 (1988).
7. J. Sunner, K. Nishizawa, P. Kebarle, *J. Phys. Chem.* **85**, 1814 (1981).
8. R. W. Taft *et al.*, *Pure Appl. Chem.* **62**, 17 (1990).
9. S. K. Burley and G. A. Petsko, *FEBS Lett.* **203**, 139 (1986). See also M. Perutz *et al.*, *J. Am. Chem. Soc.* **108**, 1064 (1986); M. Levitt and M. Perutz, *J. Mol. Biol.* **201**, 751 (1988).
10. J.-P. Changeux, A. Devillers-Thiéry, J.-L. Galzi, D. Bertrand, *TiPS* **13**, 299 (1992).
11. J. L. Sussman *et al.*, *Science* **253**, 872 (1991).
12. V. Chaturvedi, D. L. Donnelly-Roberts, T. L. Lentz, *Biochemistry* **31**, 1370 (1992); M. H. le Du, P. Marchot, P. E. Bougis, J. C. Fontecilla-Camps, *J. Biol. Chem.* **267**, 22122 (1992); T. L. Lentz, *Biochemistry* **30**, 10949 (1991).
13. S. Trumpp-Kallmeyer, J. Hoflack, A. Bruinvels, M. Hibert, *J. Med. Chem.* **35**, 3448 (1992).
14. Ab initio molecular orbital calculations (*22*) were performed with either the Gaussian 90 (*23*) or Gaussian 92 program (*24*). Calculations for benzene were carried out at the 6-31G**//6-31G** level, whereas a mixed basis set (6-31G** for C and H; STO-3G* for M⁺) was used for all of the 1:1 and 2:1 complexes. Calculations were in good agreement with full 6-31G**//6-31G** results for the 1:1 complexes of benzene with Li⁺ and Na⁺ and with experimental data for the Li⁺ and K⁺ complexes (Table 1). For the 1:1 complexes, benzene was fixed at its 6-31G**//6-31G** geometry, and the M⁺⋯benzene intermolecular separation was optimized in C_{6v} symmetry. For both models used in the calculations of the 2:1 complexes, the cation was sandwiched between two staggered, face-to-face benzene molecules (each fixed at the 6-31G**//6-31G** monomer geometry) along the vector connecting the centroids of the rings. Model I maintained D_{6d} symmetry constraints, whereas in model II, C_{6v} symmetry was maintained. These calculated gas-phase structures were then used in the solution studies.
15. All solution studies were performed at constant temperature (298 K) and pressure (1 atm) with the use of statistical perturbation theory (*25*) and the program BOSS (*26*). The complexes were treated as a single solute and placed at the center of a box 20 Å on a side containing 260 TIP3P water (*27*) molecules. Periodic boundary conditions were applied, and an 8.5 Å cutoff was used. A series of four simulations with double-wide sampling were performed for each system with 9 × 10⁵ steps of equilibration, followed by averaging over 2 × 10⁶ configurations. The OPLS parameters for benzene were optimized previously for benzene-water simulations (*28*), and parameters for the cations M⁺ had been optimized to repro-

duce relative hydration energies (*29*). The high quality of these parameters is seen in a comparison of the calculated and experimental relative aqueous solvation energies (respectively, in kilocalories per mole): Li⁺/Na⁺, 24.5 versus 23.9; Na⁺/K⁺, 17.0 versus 17.6; and K⁺/Rb⁺, 5.6 versus 5.1. However, when used to calculate gas-phase M⁺⋯benzene binding energies, the OPLS parameters give poor quantitative agreement with the ab initio results. As such, we felt it would be inappropriate to relax the M⁺⋯benzene distance during the aqueous simulations because the OPLS parameters may lead to incorrect energies or geometries. Thus, we adopted a combined approach (Fig. 1) in which the binding energies were taken from the gas-phase calculations, and statistical perturbation theory was used to determine the relative solvation energies of the various species with fixed geometries. Relative free energies of hydration were determined through stepwise perturbation of one alkali metal complex into another. Because the overall perturbations were relatively small, a fairly large step size (λ = 0.125) was used. Perturbations in the 1:1 complexes involved the mutation of Na⁺ to Li⁺ and K⁺ to Na⁺ and Rb⁺. In a similar fashion, K⁺ was changed to Li⁺, Na⁺, and Rb⁺ in the 2:1 complexes.
16. G. Eisenman, in *Symposium on Membrane Transport and Metabolism*, A. Kleinzeller and A. Kotyk, Eds. (Academic Press, New York, 1961), p. 163; ⸻ and R. Horn, *J. Membr. Biol.* **76**, 197 (1983).
17. For an alternative model emphasizing carbonyl groups as the selectivity filter, see J. Wu, *Biophys. J.* **60**, 238 (1991). For other discussions of the possible role of carbonyl oxygens in the provision of ion binding sites, see G. Eisenman and S. J. Krasne, in *MTP International Review of Science, Biochemistry Series*, C. F. Fox, Ed. (Butterworths, London, 1975), vol. 2, p. 27; G. Eisenman, O. Alvarez, J. Aqvist, *J. Inclusion Phenom. Mol. Rec-*

ognition Chem. **12**, 23 (1992).
18. Recently, it has been proposed that a cation binding site can be formed from phenylalanine side chains in the ion channel of the nicotinic ACh receptor. G. Eisenman, A. Villarroel, M. Montal, O. Alvarez, in *Progress in Cell Research*, J. M. Ritchie, P. J. Magistretti, L. Bolis, Eds. (Elsevier, New York, 1990), vol. 1, p. 195.
19. C. Miller, *Biophys. J.* **38**, 227 (1982).
20. S. R. Durell and H. R. Guy, *ibid.* **62**, 238 (1992).
21. S. Bogusz, A. Boxer, D. D. Busath, *Protein Eng.* **5**, 285 (1992).
22. W. J. Hehre, L. Radom, P. v. R. Schleyer, J. A. Pople, *Ab Initio Molecular Orbital Theory* (Wiley, New York, 1986).
23. Gaussian 90: M. J. Frisch *et al.*, Gaussian, Inc., Pittsburgh, PA, 1990.
24. Gaussian 92, revision A: M. J. Frisch *et al.*, Gaussian, Inc., Pittsburgh, PA, 1992.
25. R. W. Zwanzig, *J. Chem. Phys.* **22**, 1420 (1954); D. L. Beveridge and F. M. DiCapua, *Annu. Rev. Biophys. Biophys. Chem.* **18**, 431 (1989); W. L. Jorgensen, *J. Am. Chem. Soc.* **111**, 3770 (1989); *Acc. Chem. Res.* **22**, 184 (1989).
26. BOSS, version 2.7; W. L. Jorgensen, Yale University, New Haven, CT, 1989.
27. W. L. Jorgensen, J. Chandrasekhar, J. D. Madura, R. W. Impey, M. L. Klein, *J. Chem. Phys.* **79**, 926 (1983).
28. W. L. Jorgensen and D. L. Severance, *J. Am. Chem. Soc.* **112**, 4768 (1990).
29. J. Åqvist, *J. Phys. Chem.* **94**, 8021 (1990).
30. We thank W. Jorgensen for providing the BOSS program and for advice on parameters and H. Lester and R. MacKinnon for helpful discussions. Supported by the Office of Naval Research. Contribution no. 8759 from the Division of Chemistry and Chemical Engineering, California Institute of Technology.

20 April 1993; accepted 28 July 1993

Unusual Radar Echoes from the Greenland Ice Sheet

E. J. Rignot, S. J. Ostro, J. J. van Zyl, K. C. Jezek

Airborne radar images of part of the Greenland ice sheet reveal icy terrain whose radar properties are unique among radar-studied terrestrial surfaces but resemble those of Jupiter's icy Galilean satellites. The 5.6- and 24-centimeter-wavelength echoes from the Greenland percolation zone, like the 3.5- and 13-centimeter-wavelength echoes from the icy satellites, are extremely intense and have anomalous circular and linear polarization ratios. However, the detailed subsurface configurations of the Galilean satellite regoliths, where heterogeneities are the product of prolonged meteoroid bombardment, are unlikely to resemble that within the Greenland percolation zone, where heterogeneities are the product of seasonal melting and refreezing.

It has been known since the 1970s that radar echoes from the icy Galilean satellites are extraordinary (*1*). The radar reflectivities (*2*) of Europa, Ganymede, and Callisto are several orders of magnitude greater than those recorded for comets, the moon, the inner planets, and nonmetallic asteroids, and they show little dependence on the radar wavelength. In addition, the circular polarization ratios μ_C of the icy satellites

E. J. Rignot, S. J. Ostro, J. J. van Zyl, Jet Propulsion Laboratory, California Institute of Technology, Pasadena, CA 91109.
K. C. Jezek, Byrd Polar Research Center, Ohio State University, Columbus, OH 43210.

(*3*) exceed unity (μ_C is less than 0.4 for most other planetary targets), and their linear polarization ratios μ_L are ~0.5 (also larger than values for other planets) (*4*). More recently, radar observations of the residual south polar ice cap of Mars (*5*), portions of Titan (*6*), and polar caps on Mercury (*7*) have revealed that surfaces with high radar reflectivity and $\mu_C > 1$ exist elsewhere in the solar system.

Here we report the measurement of similarly exotic radar signatures for icy surfaces on Earth. The observations were collected in June 1991 by the National Aeronautics and Space Administration (NASA)–Jet

Propulsion Laboratory airborne synthetic-aperture radar (AIRSAR) instrument above a vast portion of the Greenland ice sheet called the percolation zone (Fig. 1), where summer melting generates water that percolates down through the cold, porous, dry snow and then refreezes in place to form massive layers and pipes of solid ice (8). The radar observations were collected simultaneously at 5.6-, 24-, and 68-cm wavelengths, and the complete scattering matrix (9) of each resolution element was measured at each radar wavelength. At the time of the radar flight, ground teams recorded the snow and firn (old snow) stratigraphy, grain size, density, and temperature (10) at ice camps in three of the four snow zones identified by glaciologists to characterize four different degrees of summer melting (8).

Figure 2 shows average values of the radar reflectivity σ_{RL}^0 (2), μ_C, and μ_L obtained from AIRSAR measurements at the Crawford Point site in the percolation zone. At 5.6 and 24 cm, σ_{RL}^0 was higher than unity at an incidence angle θ of 18°, decreased toward higher incidence angles, and showed few spatial features. At 68 cm, σ_{RL}^0 was 1/10 as large but showed kilometer-scale spatial variations. At 5.6 and 24 cm, μ_C was larger than unity for incidence angles larger than 30° and 45°, respectively, increasing to 1.6 and 1.4 at 66°. At 68 cm, μ_C was everywhere less than 0.8 and dropped as low as 0.1 in some places, with kilometer-scale spatial variations negatively correlated with those observed in the radar reflectivity images. At 5.6 cm μ_L was as large as 0.46 and at 24 cm it was 0.22, but it remained less than 0.1 at 68 cm.

In the AIRSAR scenes of the Swiss Camp and the Greenland Ice Sheet Project (GISP) II sites, at all three wavelengths corresponding values of σ_{RL}^0 were 1/10 to 1/30 of those at Crawford Point; μ_C was less than 0.4, and μ_L was less than 0.1. To our knowledge, no natural terrestrial surface other than the Greenland percolation zone shows strong echoes with $\mu_C > 1$ and $\mu_L > 0.3$ (11). However, strong echoes with large values of μ_C and μ_L have been reported for the icy Galilean satellites.

Figure 3 shows mean values of disk-integrated radar reflectivities σ_{OC}^0 and μ_C for Europa, Ganymede, Callisto, and the moon, and corresponding quantities for Greenland obtained by averaging σ_{RL}^0 and μ_C over the Crawford Point scene. The average radar properties of the percolation zone at 5.6 and 24 cm (average $\mu_C > 1$, large reflectivity) resembled those of the icy satellites at 3.5 and 13 cm. However, Greenland's average values at 24 cm were several tens of percent lower than at 5.6 cm, and μ_C was <1 at 68 cm, indicating a change in the scattering process at the longer wavelengths, whereas 70-cm estimates of μ_C for the icy satellites apparently exceeded unity (12). Also, μ_C for the percolation zone decreased significantly at incidence angles from 66° to 18°, whereas no such difference has been noticed for the icy satellites (see the caption for Fig. 3); and σ_{RL}^0 is a much stronger function of the incidence angle for the percolation zone than in the case of the icy satellites (1).

Several years ago, Zwally (13) suggested that ice inclusions could be responsible for the low emissivities measured for the percolation zone by spaceborne microwave radiometers. Since then, surface-based radio

sounding experiments, and airborne active and passive microwave measurements (14), have supported the hypothesis that volume scattering from subsurface ice layers and ice pipes is the major influence on the radar returns. Recent surface-based radar observations conducted at Crawford Point (10) at 5.4 and 2.2 cm further indicate that, at incidence angles between 10° and 70°, most of the scattering takes place in the most recent annual layer of buried ice bodies.

Figure 4 shows a representative example of firn stratigraphy in the percolation zone in early summer. Ice bodies generated from a previous summer melt are found 1.8 m below the surface. Ice layers, a millimeter to a few centimeters thick, extend at least several tens of centimeters in diameter, parallel to the firn strata (8). Ice pipes, several centimeters thick and several tens of centimeters long, are vertically extended masses reminiscent of the percolation channels that conduct meltwater down through

Fig. 2. Average values of (**A**) the OC radar reflectivity σ_{RL}^0, (**B**) the circular polarization ratio $\mu_C = \sigma_{RR}^0/\sigma_{RL}^0$, and (**C**) the linear polarization ratio $\mu_L = \sigma_{HV}^0/\sigma_{HH}^0$ for the Greenland percolation zone obtained by averaging the radar measurements recorded by AIRSAR at Crawford Point along the flight path, at 5.6, 24, and 68 cm, as a function of the incidence angle of the radar illumination, θ.

Fig. 1. Map of Greenland showing the four snow zones defined by Benson (8), the flight track of AIRSAR (continuous thick line), and the location of the Swiss Camp, Crawford Point, and the GISP II sites. Melting rarely occurs in the dry-snow zone; it forms massive, buried, solid-ice inclusions in the percolation zone; it saturates the snow with liquid water in the soaked zone; and it removes the seasonal snow cover and ablates the glacier ice in the ablation zone.
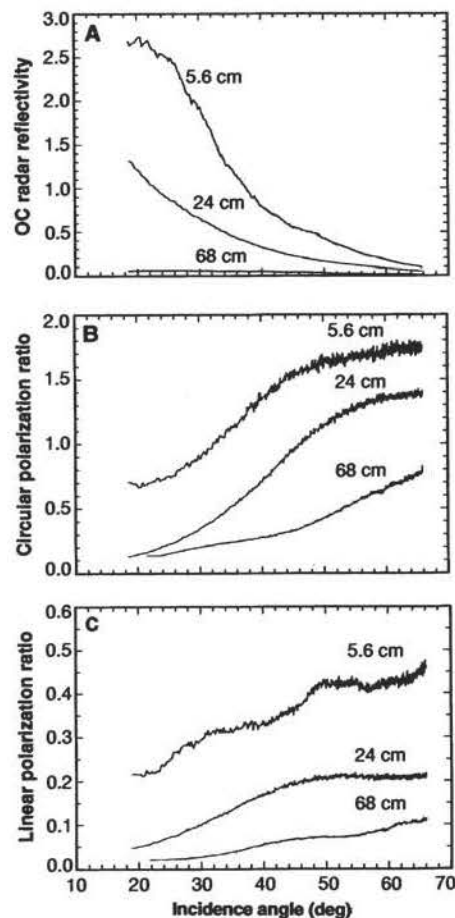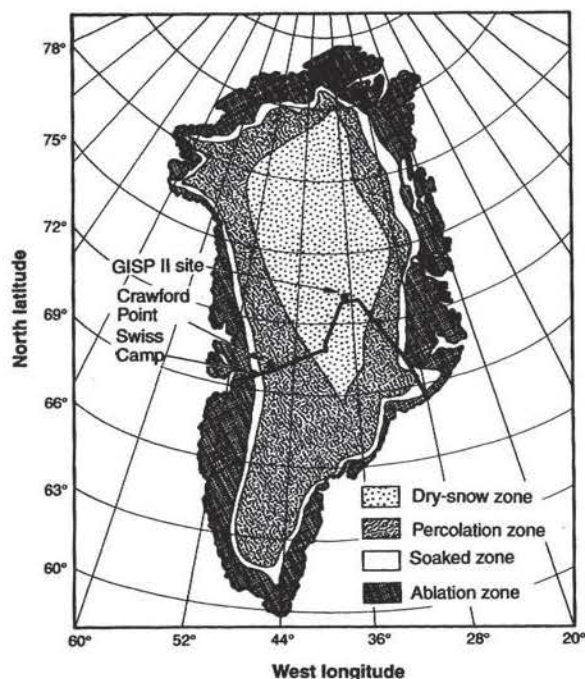
the snow during summer, feeding ice layers. The fact that radar returns measured at 68 cm are significantly weaker and have lower polarization ratios than those at 5.6 and 24 cm suggests that the discrete scatterers responsible for the radar echoes are typically less than a few tens of centimeters thick, similar to the scales of the solid-ice inclusions. The 68-cm echoes probably are dominated by single reflections from deeply buried layers of denser firn or concentrated ice bodies, whereas the 5.6- and 24-cm echoes probably are dominated by multiple scattering from the ice layers and pipes in the most recent annual layer. The relatively sharp decrease in μ_C and μ_L for $\theta < 40°$ perhaps reveals the presence of a strong, specular reflection from the ice layers at small incidence angles, which is also suggested by the strong dependence of radar reflectivity on incidence angle.

Ice layers and pipes also form in the soaked zone, but the snow there is so saturated with liquid water that the radar signals are strongly attenuated, cannot interact with the buried ice formations, and hence yield echoes with low reflectivities and polarization ratios. In the dry-snow zone, the snow is cold, porous, clean, and therefore very transparent at microwave frequencies but does not contain solid-ice scatterers that could interact with the radar signals.

For the icy satellites, no in situ measurements exist or are planned, but theoretical interpretations favor subsurface volume scattering as the source of the radar signatures. Hapke (15) suggested that the mechanism responsible for the satellites' radar behavior is the coherent backscatter effect, also known as weak localiza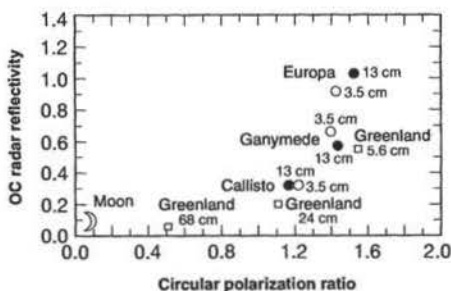tion (16), which has been observed in laboratory-controlled experiments of scattering of light from weakly absorbing, disordered random media. Coherent backscattering can theoretically produce strong echoes with $\mu_C > 1$ (the helicity of the incident polarization is preserved through multiple forward scattering) and $\mu_L \approx 0.5$, provided that (i) the scattering heterogeneities are comparable to or larger than the wavelength (17), and (ii) the relative refractive index of the discrete, wavelength-sized scatterers is smaller than 1.6 [figure 9 of (18)]. As noted by Ostro and Shoemaker (19), prolonged impact cratering of the satellites probably has led to the development of regoliths similar in structure and particle-size distribution to the lunar regolith, but the high radar transparency of ice compared with that of silicates permits longer photon path lengths and higher order scattering. Hence, coherent backscatter can dominate the echoes from Europa, Ganymede, and Callisto but contributes negligibly to lunar echoes. Similarly, the upper few meters of the Greenland percolation zone are relatively transparent (unlike the soaked zone) and, unlike the dry-snow zone, contain an abundance of solid-ice scatterers at least as large as the radar wavelength, with a relative refractive index o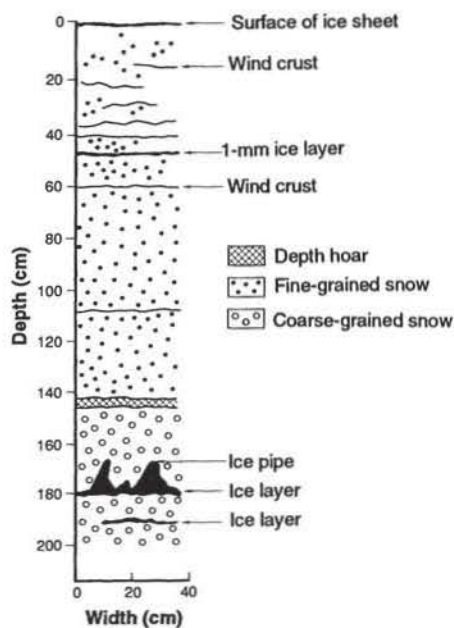f ~1.3, so coherent backscatter also can dominate the echoes there. However, it seems unlikely that the detailed subsurface configurations of the satellite regoliths, where heterogeneities result from meteoroid bombardment, would resemble that within the Greenland percolation zone, where heterogeneities are the product of seasonal melting and freezing.

We conclude that a variety of natural subsurface configurations can yield exotic radar properties. Given the increasing number of solar system surfaces (5–7) characterized by high radar reflectivities and polarization ratios, it is desirable to define as accurately as possible the physical constraints provided by the radar measurements. The Greenland percolation zone constitutes a uniquely accessible, natural laboratory for studying exotic radar scattering processes in a geological setting. Direct sampling and high-resolution, multiwavelength radar imaging of that terrain could reveal the detailed relation between radar signature and subsurface configuration, thereby furnishing a modicum of ground truth for interpreting echoes from extraterrestrial surfaces.

Fig. 3. Disk-integrated average radar properties. Points for extraterrestrial targets (circles) are averages of disk-integrated measurements at various subradar longitudes [figure 10 of (1)]. Disk-resolved echo spectra, which are equivalent to brightness scans through a slit parallel to the projected spin vector, show hardly any variation in μ_C across the satellite disks [figures 2 and 3 of (1)]. For Greenland, points (squares) are averages of measurements that span incidence angles θ from 18° to 66°. Of the projected area, 10% is at $\theta \leq 18°$ and 17% is at $\theta \geq 66°$.

Fig. 4. Snow stratigraphy at Crawford Point on the day of the AIRSAR observations. Snow grain diameters are less than 1 mm in fine-grained snow and more than 1 mm in coarse-grained snow. The average snow density is 0.2 g/cm³ in the top 40 cm and 0.4 g/cm³ between 40 and 200 cm. Wind crusts are paper-thin layers of firmly bonded, fine-grained snow. Depth hoar consists of large, skeletal crystals formed in snow strata by crystallization directly from water vapor when a temperature gradient exists in the snow.

REFERENCES AND NOTES

1. S. J. Ostro *et al.*, *J. Geophys. Res.* **97**, 18277 (1992).
2. Radar reflectivity σ^0 equals 4π times the backscattered power per steradian for unit incident flux at the target, divided by the target's projected area. Radar reflectivities for the icy Galilean satellites are mean values of disk-integrated measurements. Radar reflectivities measured by AIRSAR are single-pixel values.
3. Echoes in the same circular (SC) polarization are obtained by transmitting and receiving right circular or by transmitting and receiving left circular. That is, SC denotes either RR or LL, where R and L stand for right and left, respectively. Similarly, OC denotes either RL (right circular transmitted and left circular received) or LR. Specular reflection from a smooth surface reverses the helicity of circular polarization but preserves the direction of linear polarization. The circular and linear polarization ratios (μ_C = SC/OC, that is, RR/RL or LL/LR; and μ_L = OL/SL, where SL means same linear), of echo power in orthogonal senses, are defined so that they equal zero for back-reflection from a perfectly smooth dielectric interface. We computed μ_L values measured by AIRSAR using μ_L = HV/HH, where H and V stand for horizontal and vertical, respectively.
4. S. J. Ostro, D. B. Campbell, G. H. Pettengill, I. I. Shapiro, *Icarus* **44**, 431 (1980).
5. D. O. Muhleman, B. J. Butler, A. W. Grossman, M. A. Slade, *Science* **253**, 1508 (1991).
6. D. O. Muhleman, A. W. Grossman, B. J. Butler, M. A. Slade, *ibid.* **248**, 975 (1990); D. O. Muhleman, A. W. Grossman, M. A. Slade, B. J. Butler, *Bull. Am. Astron. Soc.* **24**, 954 (1992).
7. M. A. Slade, B. J. Butler, D. O. Muhleman, *Science* **258**, 635 (1992); J. K. Harmon and M. A. Slade, *ibid.*, p. 640.
8. C. S. Benson, *U.S. Army Snow Ice Permafrost Res. Establ. Res. Rep. 70* (Hanover, NH) (1962).
9. J. J. van Zyl and F. T. Ulaby, in *Radar Polarimetry for Geoscience Applications*, F. Ulaby and C. Elachi, Eds. (Artech House, Norwood, MA, 1990), chap. 2.
10. K. C. Jezek and S. P. Gogineni, *IEEE Geosci. Remote Sensing Soc. Newslett.* **85**, 6 (1992).
11. Double reflections from the dihedral reflectors formed by city buildings or flooded trees yield strong radar echoes, with $\mu_C > 1$ (each reflection

reverses the helicity of the polarization), but μ_L (here either HV/HH or VH/VV) is close to zero (9). Surface scattering from surfaces of root mean square height comparable to or larger than the radar wavelength, such as rough lava flows [J. J. van Zyl, C. F. Burnette, T. G. Farr, *Geophys. Res. Lett.* 18, 1787 (1991)], yields $\sigma^0_{RL} < 0.2$, $\mu_C < 0.4$, and $\mu_L < 0.2$ at all three wavelengths, for $\theta = 30°$. Volume scattering from heavily vegetated areas, such as tropical rain forest [A. Freeman, S. Durden, R. Zimmerman, in *Proceedings of the International Geoscience and Remote Sensing Symposium, Houston, Texas, May 26–29, 1992*, R. Williamson, Ed. (IEEE, New York, 1992), p. 1686] yields $\mu_C \approx 1$ and $\mu_L \approx 0.3$ at 24 and 68 cm, $\mu_C \approx 0.8$ and $\mu_L \approx 0.25$ at 5.6 cm, but $\sigma^0_{RL} < 0.1$ at all three wavelengths, for $\theta = 55°$. Unlike Greenland, none of these objects show very strong echoes with large polarization ratios.
12. D. B. Campbell, R. A. Simpson, S. J. Ostro, unpublished data.
13. H. J. Zwally, *J. Glaciol.* 18, 195 (1977).
14. C. T. Swift, P. S. Hays, J. S. Herd, W. L. Jones, V. E. Delmore, *J. Geophys. Res.* 90, 1983 (1985).
15. B. Hapke, *Icarus* 88, 407 (1990).
16. F. C. MacKintosh and S. John, *Phys. Rev. B* 37,

1884 (1988); M. P. van Albada, M. B. van der Mark, A. Lagendijk, in *Scattering and Localization of Classical Waves in Random Media*, P. Sheng, Ed. (World Scientific, Singapore, 1990), p. 97, and references therein.
17. K. J. Peters, *Phys. Rev. B* 46, 801 (1992).
18. M. I. Mishchenko, *Earth Moon Planets* 58, 127 (1992).
19. S. J. Ostro and E. M. Shoemaker, *Icarus* 85, 335 (1990). In contrast to the case of Ganymede and Callisto, few impact craters have been identified on Europa, and it is not clear whether the surficial layer of Europa is generated primarily by impacts or by internal processes, such as frost deposition.
20. We thank R. Thomas, head of the Polar Research Program at NASA Headquarters, for supporting this research; the people from the AIRSAR team for collecting and processing the SAR data used in this manuscript; J. Crawford for coordinating the AIRSAR overflights; and P. Gogineni and M. Drinkwater for discussions about Greenland glaciology. Part of this work was carried out at the Jet Propulsion Laboratory, California Institute of Technology, under contract with NASA.

28 April 1993; accepted 2 August 1993

Evidence for a Low Surface Temperature on Pluto from Millimeter-Wave Thermal Emission Measurements

S. Alan Stern,* David A. Weintraub, Michel C. Festou

Thermal continuum emission from the Pluto-Charon system has been detected at wavelengths of 800 and 1300 micrometers, and significant upper limits have been obtained at 450 and 1100 micrometers. After the subtraction of emission from Charon, the deduced surface temperature of much of Pluto is between 30 and 44 kelvin, probably near 35 to 37 kelvin. This range is significantly cooler than what radiative equilibrium models have suggested and cooler than the surface temperature derived by the Infrared Astronomy Satellite. The low temperature indicates that methane cannot be present at the microbar pressure levels indicated by the 1988 stellar occultation measurements and that the methane features in Pluto's spectrum are from solid, not gas-phase, absorptions. This result is evidence that Pluto's atmosphere is dominated by nitrogen or carbon monoxide rather than methane.

Because of Pluto and Charon's large distance from the Earth and the small sizes of these two bodies, studies of the Pluto-Charon system (PCS) are difficult (1). A number of fundamental issues in the PCS remain unresolved, such as Pluto's temperature, its bulk atmospheric composition, and the validity of its oft-cited analogous relationship to Triton. To improve the constraints on these and other important issues, we have undertaken a program of submillimeter measurements of the thermal emission from the PCS. Previous PCS thermal detections have been reported at wavelengths of 60, 100, and 1300 μm; however,

these results are discrepant (2, 3).

Our measurements were made in 1991 and 1993. The 1991 measurements were made at an effective wavelength of 1100 μm on 8 October UT with the UKT14 bolometer at the Nasmyth focus of the 15-m James Clerk Maxwell Telescope (JCMT) on Mauna Kea, Hawaii (4). The 1993 measurements were made at effective wavelengths of 450, 800, 1100, and 1300 μm on 26 January UT with the same instrument, and again at 1300 μm on 19 February UT with the MPIfR seven-channel bolometer on the 30-m Institut de Radio Astronomie Millimétrique (IRAM) telescope at Pico Veleta, Spain.

The UKT14 (5) is a sensitive ³He-cooled, single-channel bolometer with a filter wheel and variable iris. The observations reported here were made with the instrument's 65-mm-diameter circular diaphragm fully open. Sky cancellation was achieved with a chopping secondary set to

make both 40–arc sec and 60–arc sec east-west chops at a frequency of 7.8 Hz. The wavelength-dependent, half-power beam widths (HPBWs) for fully open diaphragm observations with UKT14 are given in Table 1. The MPIfR bolometer (6) is conceptually similar to the UKT14 instrument but offers the advantage of seven spatial elements arranged in a six-element daisy pattern around the central channel. Each beam has an HPBW of 12 arc sec at 1300 μm. At IRAM, the sky-chopping secondary was set to an east-west throw of 45 arc sec at a frequency of 2.0 Hz.

Accurate pointing for each observation was determined by offsetting to the calculated PCS position (7) after the use of a Gaussian fit routine to center on bright, nearby millimeter point sources. The telescope pointing errors derived from pointing checks on these nearby sources were 1 to 2 arc sec root mean square; these are small compared to the telescope beam size.

Uranus was used to calibrate the measured flux density for the 1991 JCMT and 1993 IRAM observations. Jupiter was used to calibrate the 1993 JCMT observations. We used the standard submillimeter telescope correction algorithm to compensate for finite-size effects of Uranus and Jupiter in the telescope beam. We adopted brightness temperatures for Uranus of 92.5 and 97.5 K at 1100 and 1300 μm, respectively. For Jupiter we adopted brightness temperatures of 148.5, 162.5, 170, and 170 K at 450, 800, 1100, and 1300 μm, respectively. We performed additional checks on the flux calibration and on the variability of the atmospheric optical depth at JCMT by observing several secondary calibrators [W3(OH), CRL 2688, CRL 618, and NGC 7538 IRS1, and 16293-2422] during the night at several times (8). At IRAM, telescope elevation scans called sky dips were routinely made to characterize the telluric opacity. The 1300-μm zenith opacities for our observing sessions are given in Table 1.

The maximum angular separation between Pluto and Charon is only 0.9 arc sec; hence our measurements represent the combined flux density from both Pluto and Charon (Table 1). Figure 1A depicts this set of measurements, along with Altenhoff and colleagues' 1300-μm grand average of 15 ± 1.4 mJy made in 1986. The January and February 1993 observations were of the same hemisphere of Pluto. The combination of our multiple observations gives an error-weighted detection of 10.5 ± 5.1 mJy at 1300 μm. At 800 μm we detected 33 ± 7 mJy from the PCS.

To invert our measurements and derive a temperature solution for Pluto, we first write the total flux density from Pluto and Charon as the superposition of the flux from their two gray-body Planck functions

S. A. Stern, Space Sciences Department, Southwest Research Institute, 6220 Culebra Road, San Antonio, TX 78238.
D. A. Weintraub, Department of Physics and Astronomy, Vanderbilt University, Nashville, TN 37235.
M. C. Festou, Observatoire Midi-Pyrénées, F-31400 Toulouse, France.

*To whom correspondence should be addressed.